

Systematic development of small molecules to inhibit specific microscopic steps of A β 42 aggregation in Alzheimer's disease

Johnny Habchi^{a,1}, Sean Chia^{a,1}, Ryan Limbocker^a, Benedetta Mannini^a, Minkoo Ahn^a, Michele Perni^a, Oskar Hansson^{b,c}, Paolo Arosio^a, Janet R. Kumita^a, Pavan Kumar Challa^a, Samuel I. A. Cohen^a, Sara Linse^d, Christopher M. Dobson^{a,2}, Tuomas P. J. Knowles^{a,2}, and Michele Vendruscolo^{a,2}

^aDepartment of Chemistry, University of Cambridge, Cambridge CB2 1EW, United Kingdom; ^bDepartment of Clinical Sciences, Lund University, 221 00 Lund, Sweden; ^cMemory Clinic, Skåne University Hospital, 205 02 Malmö, Sweden; and ^dDepartment of Biochemistry & Structural Biology, Center for Molecular Protein Science, Lund University, 221 00 Lund, Sweden

Edited by William A. Eaton, National Institute of Diabetes and Digestive and Kidney Diseases, NIH, Bethesda, MD, and approved November 23, 2016 (received for review September 18, 2016)

The aggregation of the 42-residue form of the amyloid- β peptide (A β 42) is a pivotal event in Alzheimer's disease (AD). The use of chemical kinetics has recently enabled highly accurate quantifications of the effects of small molecules on specific microscopic steps in A β 42 aggregation. Here, we exploit this approach to develop a rational drug discovery strategy against A β 42 aggregation that uses as a read-out the changes in the nucleation and elongation rate constants caused by candidate small molecules. We thus identify a pool of compounds that target specific microscopic steps in A β 42 aggregation. We then test further these small molecules in human cerebrospinal fluid and in a *Caenorhabditis elegans* model of AD. Our results show that this strategy represents a powerful approach to identify systematically small molecule lead compounds, thus offering an appealing opportunity to reduce the attrition problem in drug discovery.

Alzheimer's disease | amyloid- β peptide | protein misfolding | drug discovery | protein aggregation

Alzheimer's disease (AD) is, to date, an incurable neurodegenerative disorder that imposes substantial social and economic costs worldwide (1). According to the amyloid hypothesis, the aggregation of the amyloid- β peptide (A β) initiates a cascade of molecular events leading eventually to neuronal death (2–11). Because the presence of abnormal A β metabolism can be detected 10–20 years before the onset of AD (12, 13), early interventions may be possible before widespread and irreversible neurodegeneration has occurred. Although targeting A β accumulation has been pursued as a major potential therapeutic strategy against AD (14–17), no compound selected for this purpose has yet entered clinical use (18, 19).

Although these failures have raised doubts about the amyloid hypothesis (20), they can also be attributed to an incomplete knowledge of the molecular mechanisms by which the compounds tested so far affect the nucleation and growth of A β aggregates. Indeed, it has been shown that inhibiting A β aggregation without a detailed understanding of the underlying microscopic processes could affect the toxicity in unexpected ways (21, 22). For example, the inhibition of nucleation events may delay or decrease toxicity, whereas the inhibition of elongation may lead to an overall increase in toxicity (21, 22). Therefore, effective therapeutic strategies must be aimed at targeting precise microscopic steps during the A β aggregation process (21, 23–25).

We describe here the development of a systematic pipeline based on chemical kinetics to identify a pool of candidate molecules directed against the aggregation of the 42-residue form of A β (A β 42), and to understand the key chemical features responsible for their inhibitory activity.

Results and Discussion

A Quasi-Structure-Based Drug Discovery Strategy. We introduce first a quasi-structure-based drug discovery (QSBDD) strategy, which builds on the recent finding that the small molecule bexarotene

delays primary nucleation in A β 42 aggregation (22) (Fig. 1A). Because primary nuclei form only transiently during the aggregation process (21, 23, 24), it is extremely challenging to characterize their structures experimentally, making it difficult to apply to them structure-based drug discovery strategies. The structural features of these transient nuclei, however, may be shared with other biological targets of bexarotene, which was initially identified as a retinoid X receptor (RXR) agonist and approved by the US Food and Drug Administration for the treatment of cutaneous T-cell lymphoma (26). Ligands that bind RXRs and their partners, the retinoid A receptors (RARs), modulate the communication of these receptors with their intracellular environments (27, 28). The mechanisms of binding of the ligands to the RAR and RXR ligand-binding domains (LBDs) are well understood and are exploited for pharmaceutical purposes (27, 29). We took advantage of the data available on the atomic structures of the LBDs and the chemical properties of the known agonists and antagonists of RARs and

Significance

The absence of fully reproducible protein aggregation assays has contributed to the systematic failures in clinical trials for Alzheimer's disease (AD) of compounds targeting the aggregation process of the amyloid- β peptide (A β). To address this problem, we report the identification of a library of compounds against A β aggregation using a drug discovery strategy based on highly quantitative aggregation rate measurements. We then demonstrate, both in *Caenorhabditis elegans* and human cerebrospinal fluid, that this approach can systematically provide a rich variety of related small molecules to take forward into a drug discovery process. We therefore report an approach that should substantially help overcome the very high level of attrition associated with drug discovery programs for AD.

Author contributions: J.H., S.C., R.L., M.P., P.A., S.L., C.M.D., T.P.J.K., and M.V. designed research; J.H., S.C., R.L., B.M., M.A., M.P., O.H., P.A., J.R.K., P.K.C., and S.L. performed research; J.H., S.C., R.L., B.M., M.A., M.P., O.H., P.A., J.R.K., P.K.C., S.L., C.M.D., T.P.J.K., and M.V. analyzed data; and J.H., S.C., R.L., B.M., M.A., M.P., O.H., P.A., J.R.K., P.K.C., S.I.A.C., S.L., C.M.D., T.P.J.K., and M.V. wrote the paper.

Conflict of interest statement: Part of the work described in this paper has been the subject of a patent application filed by Cambridge Enterprise, a wholly owned subsidiary of the University of Cambridge (now licensed to Wren Therapeutics Ltd., where M.V. is Chief Scientific Officer; S.I.A.C., C.M.D., and M.V. are members of the Board of Directors; and S.I.A.C., S.L., C.M.D., and T.P.J.K. are consultants).

This article is a PNAS Direct Submission.

Freely available online through the PNAS open access option.

¹J.H. and S.C. contributed equally to this work.

²To whom correspondence may be addressed. Email: mv245@cam.ac.uk, tpjk2@cam.ac.uk, or cmd44@cam.ac.uk.

This article contains supporting information online at www.pnas.org/lookup/suppl/doi:10.1073/pnas.1615613114/-DCSupplemental.

RXR, and applied QSBDD by presuming that, like bexarotene, other RXR and RAR ligands may inhibit the aggregation of A β 42. We thus collected a group of 12 small molecules (Fig. 1*B*), including five RAR agonists (tamibarotene, BMS753, adapalene, CD1530, TTNPB, and Ch55), four RAR antagonists (BMS195614, LE135, MM11253, and BMS493), two RXR agonists (bexarotene and SR11237), and one RXR antagonist (UVI3003). We tested these compounds in a thioflavin-T (ThT)-based chemical kinetics assay and compared their effects on the different microscopic steps in the A β 42 aggregation reaction (Fig. 1*C*).

RAR and RXR Ligands Inhibit A β 42 Aggregation to Different Extents.

We monitored A β 42 fibril formation in vitro for 2 μ M A β 42 in the absence and presence of these small molecules. For A β 42 alone the half-time of aggregation was about 2 h under the buffer conditions used. For each compound except BMS753, we observed substantial delays in A β 42 aggregation when the compounds were included at a concentration of 6 μ M [3 molar equivalents (M eq)] (Fig. 2*A*). In most cases, the delays were greater than those assessed for bexarotene, and five of the 12 molecules (MM11253, BMS493, adapalene, CD1530, and LE135) inhibited the aggregation of A β 42 completely over 10 h of observation (Fig. 2*A*). These five compounds were very effective in delaying the aggregation of A β 42 even at substoichiometric ratios (0.5 M eq; Fig. 2*B*). To investigate these effects further and to exclude possible interferences of the compounds with ThT binding to A β 42 fibrils and the fluorescence measurements, we probed the quantities of A β 42 fibrils at 12 time points during the aggregation reaction in the absence and presence of the small molecules using a dot-blot assay with an A β 42 fibril-specific antibody (OC; see *Methods*) (Fig. 2*C* and *D* and Fig. S1). The delay induced by the small molecules in the dot-blot assay was found to be identical within experimental error to the delay observed in the ThT-based assay.

We subsequently classified these molecules according to their efficacy in inhibiting A β 42 aggregation. The intensities of the dot blots (Fig. 2*C* and *D*) were quantified and normalized against the intensity of A β 42 alone. The values at two early time points were plotted against the half-times derived from the ThT-based kinetics (Fig. 2*E* and *F*), resulting in a linear correlation, showing the high degree of consistency between the two assays. This analysis allowed the classification of the RAR and RXR ligands in two sets according to the extent of the delay induced in A β 42 aggregation (Fig. 2*E* and *F*). Set A consists of seven molecules showing an effect at 3 M eq similar to or greater than the effect of bexarotene (Fig. 2*E*, light green), and set B consists of five molecules that completely inhibited A β 42 aggregation for at least 10 h at 3 M eq. We then analyzed the effects of these molecules at substoichiometric concentrations by both assays (Fig. 2*F*, light orange). UVI3003 was identified as the most effective molecule within set A, delaying by more than fourfold the aggregation reaction, whereas MM11253 and adapalene were found to be the most effective molecules within set B, because the aggregation of 2 μ M A β 42 was delayed by at least threefold at a concentration half of the concentration of A β 42. Furthermore, RAR and RXR ligands inhibited A β 42 reaction in a concentration-dependent manner, with set B molecules showing efficacy at concentration ratios as low as 0.2 (Fig. S2). The only molecule that did not show any effect on A β 42 aggregation was BMS753, even when present at 5 M eq (Fig. S3).

RAR and RXR Ligands Inhibit Primary and Secondary Pathways.

We next carried out a quantitative analysis of the effects of the molecules by matching the experimental aggregation profiles to kinetic curves obtained by using the rate laws derived from a master equation that relates the time evolution of fibril formation to the rate constants of the different microscopic events (21, 24, 25). In this approach, the aggregation profiles in the presence

of an inhibitor are described by introducing into the rate laws suitable perturbations to each of the microscopic rate constants evaluated in the absence of the inhibitor. The modifications of the rate constants required to describe the aggregation profiles in the presence of different concentrations of inhibitor are then indicative of the specific process affected by the presence of the compound (21).

At low concentrations of small molecules, the data are extremely well described when the primary pathways [as expressed by the product of the of primary nucleation and rate of elongation ($k_n k_+$)] are specifically decreased at less than a 3 M eq of set A and less than 0.5–1 M eq of set B molecules, where k_+ is the rate constant of fibril elongation and k_n is the rate constant for primary nucleation (Fig. 3*A–C* and *F–H* and Figs. S4 and S5). By contrast, at higher concentrations of small molecules, the data are consistent with a decrease in the rate constants of both primary ($k_n k_+$) and secondary ($k_2 k_+$) pathways, where k_2 is the rate constant of surface-catalyzed secondary nucleation. All kinetic curves were then compared with simulations where both primary and secondary pathways were decreased concomitantly, and the rates of both pathways were plotted against the concentration of small molecules (Fig. 2*A–J* and Figs. S4 and S5). This analysis revealed that set A and set B molecules can affect both nucleation pathways in A β 42 aggregation (Fig. 2*A–J* and Figs. S4 and S5).

To quantify the effects of the small molecules on A β 42 aggregation further, we examined the increase in ThT fluorescence at the end of the reaction, finding similar values in all cases (Figs. S4*H* and S5*F*). These results suggest that a similar fibril mass concentration is formed irrespective of whether or not the small molecules are present, in agreement with the dot-blot assays. In addition, the effect of the small molecules on the aggregation kinetics of A β 42 was found to be mainly determined by the molar ratio of the small molecules with respect to A β 42 rather than by its total absolute concentration (Fig. S6*A–C*), thus implying that our experiments are conducted above the K_d for the relevant interactions. Based on these results, given that the concentration of A β 42 is much lower in vivo than that used here in vitro, we would expect that much lower concentrations of the compounds could be required to affect the rate constants of A β 42 aggregation to the same extent, although the molar ratio might need to be increased in the concentration range below the value of K_d .

Furthermore, to rule out any possible interference of the small molecules on the aggregation pathway of A β 42, such as a stabilization of nonfibrillar aggregates, we used transmission electron microscopy (TEM) to image the A β 42 species formed at the end of the aggregation reactions in the absence and presence of two representative molecules from sets A and B, namely, BMS195614 and LE135 (Fig. S6*E* and *F*). In agreement with our previous atomic force microscopy findings on the effect of bexarotene on the aggregation kinetics of A β 42 (22), the TEM images showed that similar A β 42 fibrillar species are formed at the end of the aggregation reactions.

RAR and RXR Ligands Inhibit Secondary Pathways to Different Extents.

To explore further the effects of the molecules on distinct steps of the secondary pathways further (i.e., on the surface-catalyzed secondary nucleation and elongation steps), we carried out an additional series of kinetic measurements in the presence of the different compounds and various concentrations of preformed fibril seeds. For about 10% of preformed fibrils, the primary and secondary nucleation steps are bypassed and the formation of mature fibrils is greatly accelerated by elongation reactions promoted by the fibril seeds (Fig. S7). Under these conditions, set A molecules did not affect the aggregation kinetics of 2 μ M A β 42 even at a concentration of 5 M eq relative to the peptide (Fig. 4*A*), whereas the corresponding aggregation process under unseeded conditions was slowed by at least a factor of 3 (Fig. 2*A*), strongly indicating that the set A compounds have no effect on elongation.

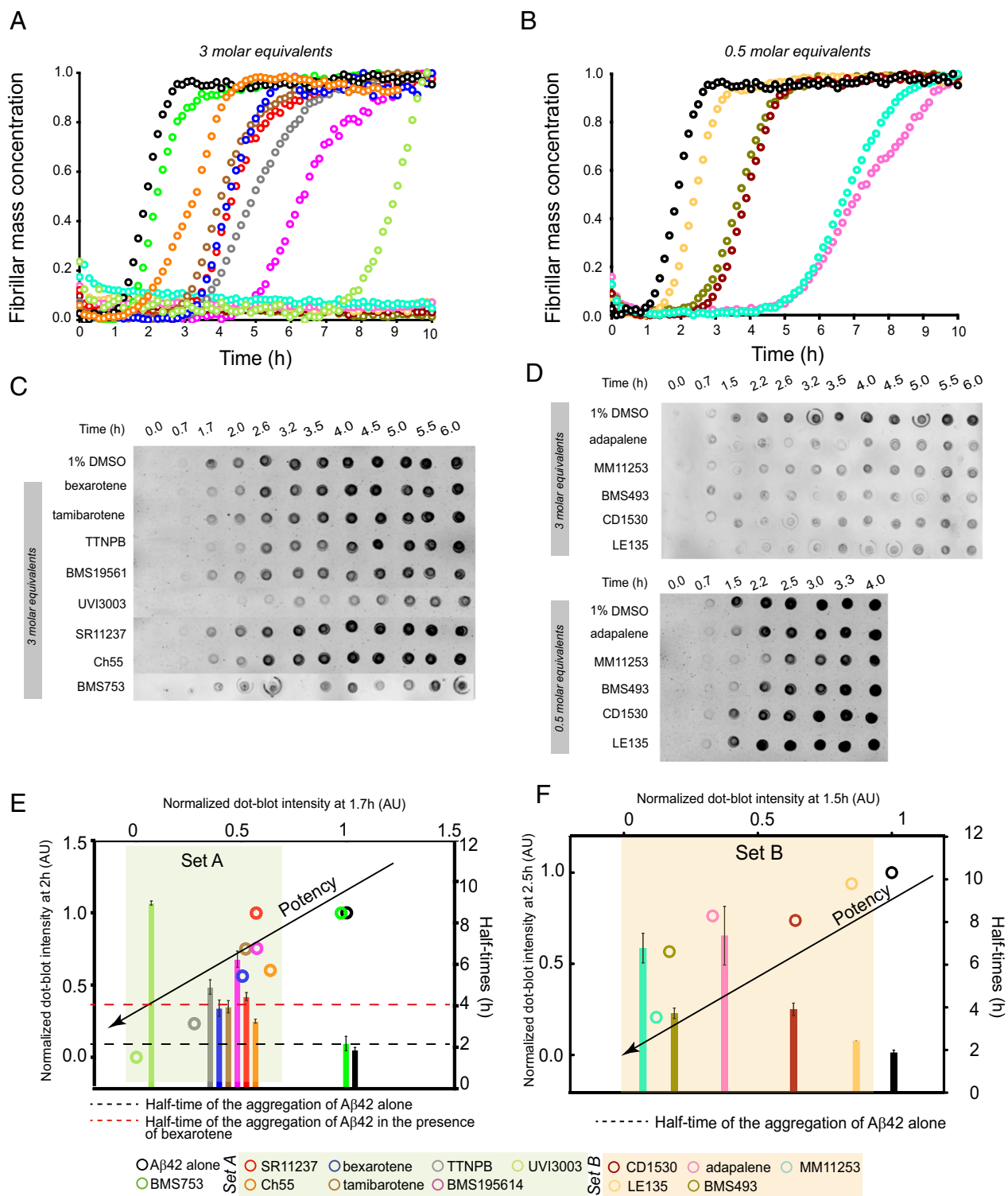


Fig. 2. RAR and RXR ligands affect A β 42 aggregation to different extents. (A) Kinetic profiles of the aggregation of a 2 μ M solution of A β 42 in the absence and presence of 3 M eq of RAR and RXR ligands, shown in different colors. Note that A β 42 did not aggregate within 10 h in the presence of five of the 13 molecules, seen as flat lines. (B) Kinetic profiles of 2 μ M A β 42 aggregation in the absence and presence of substoichiometric ratios of the five molecules that are shown as flat lines in A. (C and D) Comparative time course of the formation of 2 μ M A β 42 fibrils in the absence and presence of 3 M eq of the small molecules using a dot-blot assay. A β 42 in (D, Top) did not aggregate in the presence of 3 M eq of adapalene, MM11253, BMS493, CD1530, and LE135; therefore, the aggregation kinetics of 2 μ M A β 42 were repeated in the presence of substoichiometric quantities of the same molecules (0.5 M eq) (D, Bottom). The plots show, as histograms, the half-times of the aggregation reactions of A β 42 from A and B and, as open circles, the correlation between the normalized dot-blot intensities with respect to the correlation in the presence of 1% DMSO at 1.6 h and 2 h (E) and 1.5 h and 2.5 h (F) of the aggregation reactions from C and D. The molecules were separated into two sets according to their potency, which was evaluated based on the extent of the delay that they induced in A β 42 aggregation. (E) Set A (highlighted in light green) contains the molecules showing an effect similar to or greater than that of bexarotene (the half-time of A β 42 aggregation in the absence and presence of bexarotene are highlighted with dotted black and red lines, respectively). AU, arbitrary units. (F) Molecules classified as set B (highlighted in light orange) inhibited the aggregation of A β 42 completely within 10 h in the presence of 3 M eq of the small molecules.

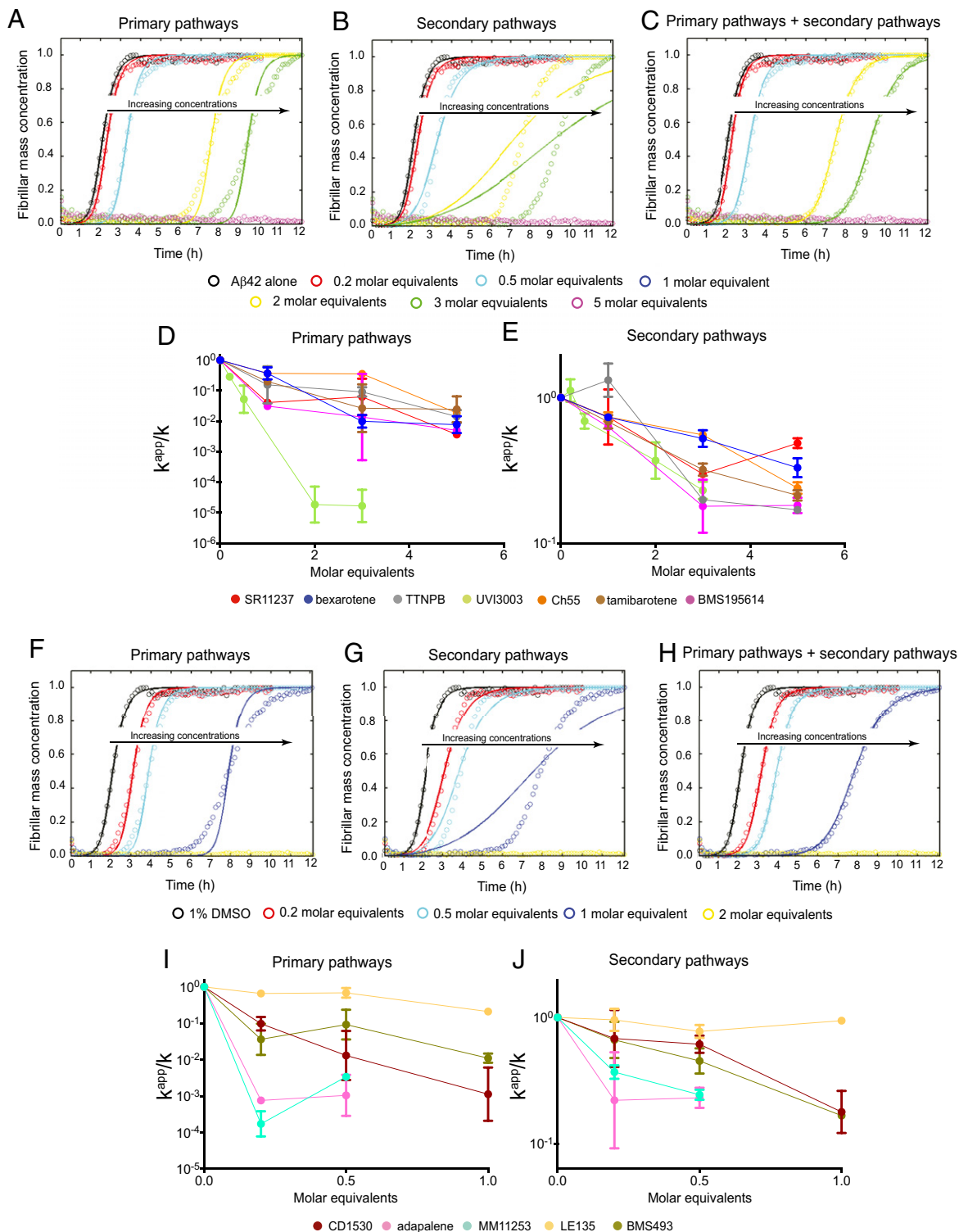


Fig. 3. Characterization of the effects of set A and set B molecules on A β 42 aggregation using quantitative chemical kinetics. (A–C) Kinetic profiles of the aggregation of 2 μ M A β 42 in the absence and presence of either 1% DMSO (black) or 0.2 (red), 0.5 (cyan), 1 (blue), 2 (yellow), 3 (green), or 5 (magenta) M eq of UVI3003, a representative molecule of set A. The solid lines show predictions for the resulting reaction profiles when primary pathways (A, $k_n k_+$), secondary pathways (B, $k_2 k_+$), or both pathways (C) are inhibited by UVI3003. The abbreviation k_n is the rate of primary nucleation, k_+ is the rate of elongation, and k_2 is the rate of secondary nucleation. Only predictions when both pathways are inhibited fit the experimental data well. The dependence of the apparent reaction rate constants (k^{app}) of primary pathways (D, $k_n k_+$), and secondary pathways (E, $k_2 k_+$), as derived from Fig. S4, is shown with increasing concentrations of small-molecule inhibitors. In each case, k represents either $k_n k_+$ (primary pathways) or $k_2 k_+$ (secondary pathways). (F–H) Kinetic profiles of the aggregation of a 2 μ M A β 42 solution in the absence and presence of either 1% DMSO (black) or 0.2 (red), 0.5 (cyan), 1 (blue), or 2 (yellow) M eq of CD1530, a representative molecule of set B. The solid lines show predictions for the resulting reaction profiles when primary pathways (F, $k_n k_+$), secondary pathways (G, $k_2 k_+$), or both pathways (H) are inhibited by CD1530. Only predictions when both pathways are inhibited fit the experimental data well. Dependences of the apparent reaction rate constants of primary pathways (I, $k_n k_+$) and secondary pathways (J, $k_2 k_+$), as derived from Fig. S5, is shown with increasing concentrations of small-molecule inhibitors.

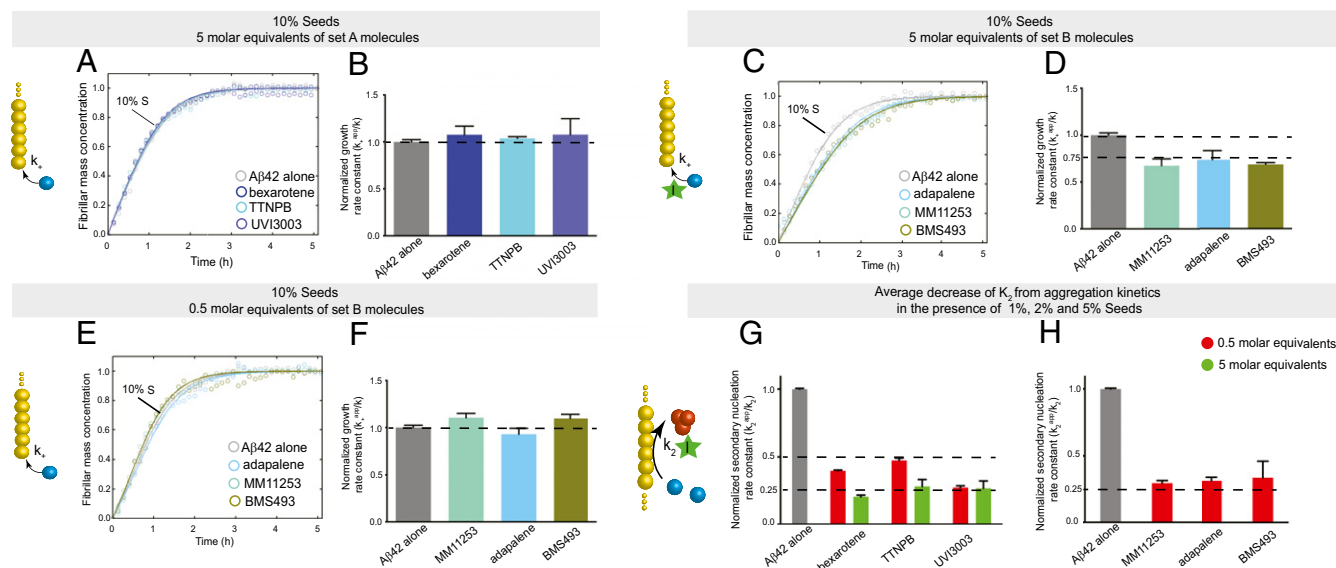


Fig. 4. Characterization of the effects of set A and set B molecules on the secondary pathways of A β 42 aggregation. (A) Kinetic aggregation profiles of a 2 μ M A β 42 solution in the presence of 10% of preformed seeds in the absence (gray) or presence of 5 M eq of bexarotene (blue), TTNPB (cyan), and UVI3003 (orchid). Under these conditions, elongation of the fibrils is the dominant mechanism. (B) Normalized growth rate constants derived from the fitted curves in A in the presence of 10% of preformed seed fibrils; these results show that set A molecules do not detectably affect the elongation rates of A β 42 aggregation. (C) Kinetic profiles of the aggregation of a 2 μ M A β 42 solution in the presence of 10% of preformed seeds in the absence (gray) or presence of 5 M eq of MM11253 (green), adapalene (blue), and BMS493 (moss green); under these conditions, elongation of the fibrils is the dominant mechanism. (D) Normalized growth rate constants derived from the fitted curves in C in the presence of 10% of preformed seed fibrils; these results show that set B molecules affect the elongation rates of A β 42 aggregation at 5 M eq. (E) Kinetic profiles of the aggregation of a 2 μ M A β 42 solution in the presence of 10% of preformed seeds in the absence (gray) or presence of 0.5 M eq of MM11253 (green), adapalene (blue), and BMS493 (moss green); under these conditions, elongation of the fibrils is the dominant mechanism. (F) Normalized growth rate constants derived from the fitted curves in E in the presence of 10% of preformed seed fibrils; these results show that set B molecules at 0.5 M eq do not affect the elongation rates of A β 42 aggregation. Effect of 0.5 and 5 M eq of set A (G; bexarotene, TTNPB, and UVI3003) and set B (H; MM11253, adapalene, and BMS493) on the rates of the surface-catalyzed secondary nucleation (k_2). The rate constants were obtained from the aggregation kinetics of a 2 μ M A β 42 solution in the presence of 1%, 2%, and 5% of preformed seeds (Figs. S8 and S9), where primary nucleation is negligible and surface-catalyzed secondary nucleation contributes ~35%, 60%, and 80%, respectively, of the total quantity of fibrils formed, according to the simulations shown in Fig. S7. The quantitative parameters were obtained from the fitted curves in Figs. S7 and S8. The observed effects could only be due to decreasing the rate constants of surface-catalyzed secondary nucleation because elongation is not affected by the compounds under these conditions.

This interpretation was confirmed quantitatively by deriving the growth rate constants from the kinetic curves in the absence and presence of each of the set A molecules (Fig. 4B). The molecules in set B decreased the growth rate constants by about 25% at a concentration fivefold greater than the peptide (Fig. 4C and D), thus explaining the increased delay in A β 42 aggregation in the presence of set B molecules with respect to A β 42 aggregation in set A molecules. Additionally, at substoichiometric concentrations (e.g., a concentration ratio of 0.5 compared with the peptide), no effects were observed with any of the set B molecules on the elongation of A β 42 fibrils, thus indicating that the inhibition of the elongation step requires higher concentrations of small molecules than the nucleation steps (Fig. 4E and F).

To obtain a more complete comparative assessment on the effects of set A and set B molecules on the secondary pathways of A β 42 aggregation, we measured the aggregation kinetics of a 2 μ M A β 42 sample in the presence of 1%, 2%, and 5% of fibril seeds (Figs. S7 and S8). Simulations based on the experimental kinetic curves show that primary nucleation is completely bypassed when even the smallest ratios (1%) of preformed seeds are introduced in the solution. By contrast, surface-catalyzed secondary nucleation and elongation contribute in different ways to the overall kinetics, with the contribution of elongation becoming more significant with increasing seed concentrations (Fig. S7). Hence, following the aggregation kinetics of A β 42 using different seed concentrations allows decoupling of the secondary pathways into the surface-catalyzed secondary nucleation and elongation steps. Such decoupling is crucial to char-

acterize the effects of the small molecules on the individual microscopic steps; these effects might not otherwise be detected directly from the aggregation kinetics in the absence of preformed seeds (23, 25). Data at 1% and 5% of seeds showed a concentration-dependent inhibition of secondary pathways (i.e., a reduction of k_2k_+) of A β 42 aggregation in the presence of both sets A and B of compounds (Fig. 4G and H and Figs. S8 and S9). In the case of set A molecules, the decrease at 0.5 and 5 M eq could be attributed solely to a decrease in the rate constant of the surface-catalyzed secondary nucleation (i.e., k_2) because no effect could be observed on the elongation of the fibrils (i.e., k_+) at molar equivalents as high as 5 (Fig. 4A and B). The rate constants could be derived quantitatively from the kinetic curves and were found to be decreased by about 50% and 75% in the presence of 0.5 and 5 M eq of set A molecules, respectively.

Although the elongation of fibrils is essentially unaffected by the set A molecules, these compounds have large effects on the nucleation steps in A β 42 aggregation. The effects on secondary nucleation were very pronounced in the presence of low concentrations of the molecules, further supporting the key role of this process in promoting the catalytic cycle in A β 42 aggregation (24). By contrast, for set B molecules, the effects on the secondary nucleation rate constant could be quantified only under the conditions where elongation was not affected (i.e., in the presence of 0.5 M eq of the small molecules). Set B molecules were found to be significantly more effective in inhibiting secondary nucleation in A β 42 aggregation than set A molecules, with the decrease being as high as

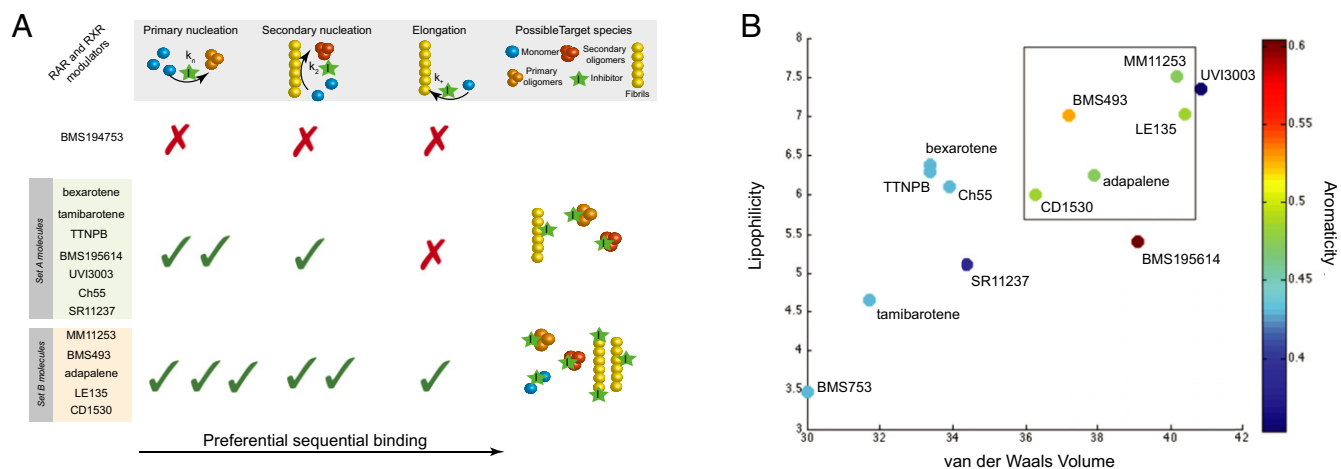


Fig. 5. Characteristic chemical features of the small molecules found in this study to inhibit A β 42 aggregation. (A) Summary of the effects of the tested molecules on the microscopic steps of A β 42 aggregation and of the possible target species. (B) Correlation between lipophilicity, van der Waals volume, and aromaticity of the small molecules and their contribution to the relative potency of the molecules. The box in the figure includes the molecules from set B.

75% at 0.5 M eq, thus further confirming the higher potency of set B molecules with respect to the potency of set A molecules.

Characteristic Chemical Features of Small Molecules Are Required to Inhibit Specific Microscopic Steps in A β 42 Aggregation.

The observation that set A and set B molecules affect different microscopic steps in the aggregation of A β 42 could result from the interactions of the small molecules with different A β 42 species formed along the aggregation pathway (Fig. 5A), because inhibiting both primary and secondary nucleation could result from binding of the small molecules to primary and secondary nuclei and/or, in the latter case, fibril surfaces. On the other hand, considering the qualitative correlation between the inhibited processes and the target species, one might expect that the inhibition of A β 42 aggregation by set B molecules may, in principle, originate mainly

from interactions with A β 42 monomers. Indeed, because the monomeric species of A β 42 are involved in all microscopic events that underlie its aggregation, as seen in Fig. 5A (i.e., primary nucleation, surface-catalyzed secondary nucleation, elongation), one possible scenario, in which the small molecule inhibits all three steps, is that it binds to the common species (i.e., the monomer in all cases). We examined the likelihood of this scenario in a quantitative manner by attempting a description of the kinetic data where the small molecules sequester monomeric species of A β 42. In this case, the kinetic curves in the presence of increasing concentrations of the small molecules would correspond to a decreased concentration of A β 42 available to aggregate. We found, however, that this assumption is incorrect because the kinetic data could not be accurately described (Fig. S10 A–F). Furthermore, NMR spectroscopy measurements showed no significant perturbations of the chemical

Measurements of the effect of selected molecules on A β 42 aggregation under physiological conditions

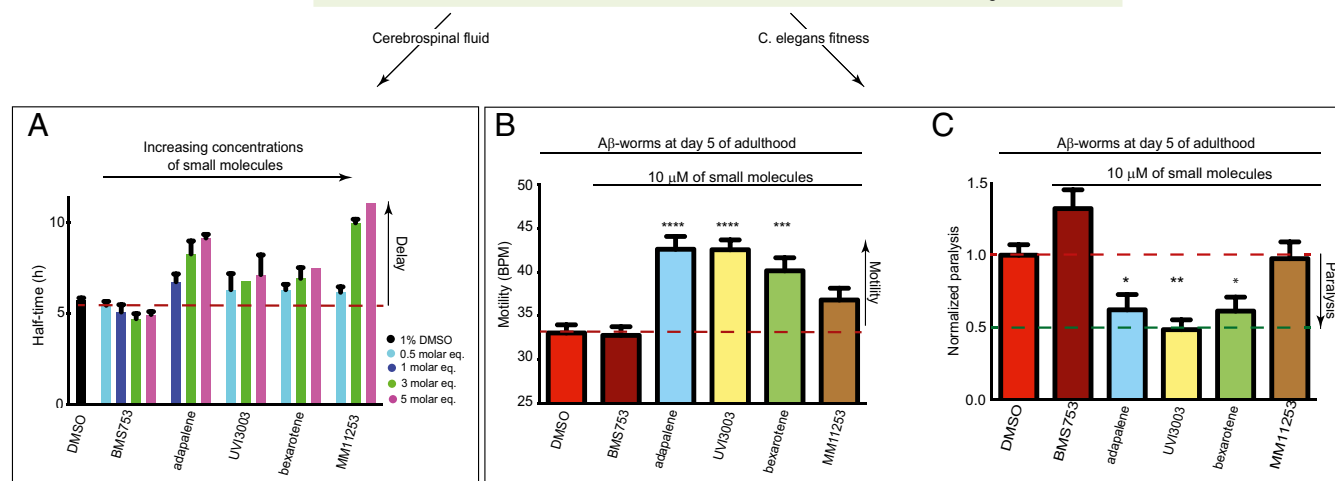


Fig. 6. Characterization of the effects of small molecules in CSF solutions and in a *C. elegans* model of A β 42-mediated cytotoxicity. (A) Dose-dependent effects of selected molecules from set A and set B on the half-times of the aggregation reaction of A β 42 in 66% CSF solutions. Measurements of the effects of a 10 μ M solution of selected molecules from set A and set B in 0.6% DMSO on the frequency of body bends (B) and the paralysis rate (C) at day 5 of adulthood of the A β 42-worm model. Experimental data are averaged over three separate experiments ($n_{\text{tot}} \approx 800$ worms). The efficacy of these compounds was determined based on their ability to increase the fitness of the worms with respect to untreated A β 42 worms. Statistics were determined using one-way ANOVA against 0.6% DMSO motility: * $P < 0.05$; ** $P < 0.01$; *** $P < 0.001$; **** $P < 0.0001$. Error bars represent the SEM. BPM, bends per minute.

shifts and the resonance intensities in the heteronuclear single quantum coherence spectra of a 25 μM sample of ^{15}N -labeled monomeric A β 42 before and after the addition of each of the set B molecules and of UVI3003, the most effective molecule of set A, as a control (Fig. S10 G–L). These observations indicate that set B molecules are likely to bind both primary and secondary nuclei, and the fibril surfaces and ends, but not monomers.

Unlike set A molecules, set B molecules were found to inhibit all three major steps in A β 42 aggregation, with the effects on the primary and secondary nucleation steps being greater than the effects of the set A molecules. It is thus of great significance to identify the chemical features responsible for these differences, because such features can at least in principle enable the rational design of molecules against specific microscopic steps in A β 42 aggregation. From an analysis of the molecular properties of the small molecules, we selected two parameters: the lipophilicity, defined as the Ghose–Crippen octanol/water coefficient (30), and the steric bulk, defined as the sum of the atomic van der Waals volumes (31). We identified a linear correlation between these two parameters that largely accounts for the efficacy of all of the small molecules (Fig. 5B). The greater the lipophilicity and the steric bulk, the higher is the potency of the small molecule, with very low values of their sum corresponding to the complete abolition of the effects of a molecule, as in the case of BMS753. Strikingly, UVI3003, the most potent molecule in set A, was found to possess similar lipophilicity and steric bulk values to those values in set B molecules, and, accordingly, a similar potency is predicted from the correlation in Fig. 5B. Although no effect was observed on the elongation step, UVI3003 inhibits both the primary and secondary nucleation steps to a similar degree to the molecules in set B. These results suggest that the lipophilicity and steric bulk describe well the effects of small molecules on the primary and secondary nucleation steps, but not on the elongation step. To decipher the chemical features of the small molecules responsible for inhibiting the elongation step, we considered an additional parameter: the value of the relative aromaticity of the small molecules, defined as the ratio of the number of aromatic atoms to the total number of atoms. We thus found that a high aromaticity value confers the ability to inhibit the elongation of A β 42 fibrils (Figs. 4 C and D and 5B). Indeed, all of the set B molecules have aromaticity values greater than the aromaticity values of the set A molecules.

RAR and RXR Ligands Inhibit A β 42 Aggregation in CSF Solutions and Rescue A β 42-Mediated Dysfunction in a *C. elegans* Model. We next explored if the small molecules retard A β aggregation under more physiologically relevant conditions. We therefore monitored these effects on the aggregation kinetics of A β 42 in human cerebrospinal fluid (CSF). CSF caused a concentration-dependent retardation of A β 42 aggregation, suggesting that A β 42 aggregation is slower in this fluid, in line with previous results (32) (Fig. S11A). We then investigated the effects of selected small molecules from set A (bexarotene and UVI3003) and set B (MM11253 and adapalene), and from BMS753 as a negative control, under conditions where the effect of CSF is close to maximal (i.e., 66%) (Fig. S11B). We found that under these conditions, all selected small molecules, except for BMS753 (Fig. S12), significantly delayed the aggregation kinetics in a concentration-dependent manner similar to what has been observed in buffer (Fig. 6A and Fig. S13).

We further evaluated the effects of the same small molecules in a *C. elegans* model of A β 42-mediated dysfunction, denoted GMC101 (termed the A β -worm model) (22). In this model, A β 42 is expressed in body wall muscle cells, where it forms aggregates and results in progressive paralysis (22). We assessed the effects of the small molecules on the fitness of the worms in terms of the frequency of body bends (i.e., motility) and the rate of their paralysis. Because all molecules from both sets A and B have significant effects on the nucleation steps of A β 42 aggregation, we added them at the larval stages of the *C. elegans* life

cycle (i.e., L4), where no aggregation of A β 42 has occurred yet. At day 5 of worm adulthood, where the fitness of the A β -worms was significantly decreased compared with the control-worms (Fig. S14A), the selected small molecules restored the motility of the worms substantially, except for the negative control BMS753 (Fig. 6B), in a concentration-dependent manner (Fig. S14B). These results are similar to the results observed in vitro and in human CSF. In addition, no selected molecules showed any significant effect in a wild-type worm model that does not express A β 42, N2 (termed the control-worm model) (Fig. S14C). These data suggest that the small molecules restore the motility of the A β -worms by specifically inhibiting the aggregation of A β 42. Indeed, the level of aggregates was measured in A β -worms in the absence and presence of bexarotene using the fluorescence intensity of the amyloid-specific dye NIAD-4, and was found to be similar to the level of aggregates of the control-worms in the presence of bexarotene, where no aggregates could be detected (22). We found that all selected small molecules decreased the rate of paralysis of the A β worms, except for MM11253. This finding is in agreement with the unexpected lower increase in the motility of the A β -worms in the presence of MM11253, which was found to be extremely potent in vitro. Because no MM11253-related toxicity could be observed, as judged from the absence of any effect on the fitness of control worms (Fig. S14C), this finding is likely to be due to a lower half-life of this molecule in worms compared with adapalene, bexarotene, and UVI3003 (Fig. 6C). In any case, all molecules that have shown an effect on the aggregation of A β 42 in vitro are also able to restore the fitness of the A β -worms, thus further supporting the power of the kinetic assay in drug discovery. The effects of the small molecules are also readily detectable under stress conditions, because bexarotene (set A) and adapalene (set B) restore the fitness, in terms of motility (Fig. S15A) and paralysis (Fig. S15B), of A β -worms that were exposed to temperature-induced stress (Fig. S15).

Conclusions

We have described a drug discovery approach based on quantitative chemical kinetics to identify small molecules that target specific microscopic steps in A β 42 aggregation. The results that we have obtained suggest that this approach is highly effective for drug discovery against protein misfolding diseases because, unlike other available approaches not based on chemical kinetics, it provides quantitative descriptions of the inhibitory process, thus making it possible to control and modulate the onset of the aggregation in vitro. In addition, the molecules that we have described, particularly those in set B, are expected to have a greater effect not only on the onset of aggregation but also on the proliferation of the A β 42 oligomers produced through surface-catalyzed secondary nucleation. Therefore, targeting such a process, which is largely responsible for the production of toxic A β 42 species (23, 24), should provide an effective means for the development of treatments against the progression of AD. Given the connection between the aggregation of A β 42 and AD, and the fact that the typical age for the onset of sporadic AD is around 65 years, even a small delay in A β aggregation may postpone the onset by long enough to reduce the risk of developing AD significantly. Thus, inhibiting the nucleation steps in A β 42 aggregation should result in a delay and reduction in the formation of toxic A β 42 oligomers (22, 23), which are considered central to the pathology of AD; therefore it is likely to be a promising route to preventing AD. We anticipate that the combination of QBSDD and kinetics-based drug discovery will allow the screening of databases for the identification of pools of potent small molecules against A β 42 aggregation. This approach will also enable the rational design of candidate molecules bearing the chemical features that are crucial for inhibiting specific microscopic steps of the protein aggregation reaction, and that possess good drug pharmacokinetic characteristics.

1. Alzheimer's Association (2012) 2012 Alzheimer's disease facts and figures. *Alzheimers Dement* 8(2):131–168.
2. Hardy J, Selkoe DJ (2002) The amyloid hypothesis of Alzheimer's disease: Progress and problems on the road to therapeutics. *Science* 297(5580):353–356.
3. Selkoe DJ (2003) Folding proteins in fatal ways. *Nature* 426(6968):900–904.
4. Haass C, Selkoe DJ (2007) Soluble protein oligomers in neurodegeneration: Lessons from the Alzheimer's amyloid beta-peptide. *Nat Rev Mol Cell Biol* 8(2):101–112.
5. Dobson CM (2003) Protein folding and misfolding. *Nature* 426(6968):884–890.
6. Knowles TP, Vendruscolo M, Dobson CM (2014) The amyloid state and its association with protein misfolding diseases. *Nat Rev Mol Cell Biol* 15(6):384–396.
7. Holtzman DM, Morris JC, Goate AM (2011) Alzheimer's disease: The challenge of the second century. *Sci Transl Med* 3(77):77sr1.
8. Tanzi RE, Bertram L (2005) Twenty years of the Alzheimer's disease amyloid hypothesis: a genetic perspective. *Cell* 120(4):545–555.
9. Karran E, Mercken M, De Strooper B (2011) The amyloid cascade hypothesis for Alzheimer's disease: An appraisal for the development of therapeutics. *Nat Rev Drug Discov* 10(9):698–712.
10. Huang Y, Mucke L (2012) Alzheimer mechanisms and therapeutic strategies. *Cell* 148(6):1204–1222.
11. Selkoe DJ, Hardy J (2016) The amyloid hypothesis of Alzheimer's disease at 25 years. *EMBO Mol Med* 8(6):595–608.
12. Bateman RJ, et al.; Dominantly Inherited Alzheimer Network (2012) Clinical and biomarker changes in dominantly inherited Alzheimer's disease. *N Engl J Med* 367(9):795–804.
13. Buchhave P, et al. (2012) Cerebrospinal fluid levels of β -amyloid 1–42, but not of tau, are fully changed already 5 to 10 years before the onset of Alzheimer dementia. *Arch Gen Psychiatry* 69(1):98–106.
14. Bieschke J (2013) Natural compounds may open new routes to treatment of amyloid diseases. *Neurotherapeutics* 10(3):429–439.
15. Chen J, Armstrong AH, Koehler AN, Hecht MH (2010) Small molecule microarrays enable the discovery of compounds that bind the Alzheimer's A β peptide and reduce its cytotoxicity. *J Am Chem Soc* 132(47):17015–17022.
16. Lansbury PT, Lashuel HA (2006) A century-old debate on protein aggregation and neurodegeneration enters the clinic. *Nature* 443(7113):774–779.
17. Necula M, Kaye R, Milton S, Glabe CG (2007) Small molecule inhibitors of aggregation indicate that amyloid beta oligomerization and fibrillization pathways are independent and distinct. *J Biol Chem* 282(14):10311–10324.
18. Cummings JL, Morstorf T, Zhong K (2014) Alzheimer's disease drug-development pipeline: Few candidates, frequent failures. *Alzheimers Res Ther* 6(4):37.
19. Karran E, Hardy J (2014) A critique of the drug discovery and phase 3 clinical programs targeting the amyloid hypothesis for Alzheimer disease. *Ann Neurol* 76(2):185–205.
20. De Strooper B, Karran E (2016) The cellular phase of Alzheimer's disease. *Cell* 164(4):603–615.
21. Arosio P, Vendruscolo M, Dobson CM, Knowles TP (2014) Chemical kinetics for drug discovery to combat protein aggregation diseases. *Trends Pharmacol Sci* 35(3):127–135.
22. Habchi J, et al. (2016) An anticancer drug suppresses the primary nucleation reaction that initiates the production of the toxic A β 42 aggregates linked with Alzheimer's disease. *Sci Adv* 2(2):e1501244.
23. Cohen SI, et al. (2015) A molecular chaperone breaks the catalytic cycle that generates toxic A β oligomers. *Nat Struct Mol Biol* 22(3):207–213.
24. Cohen SI, et al. (2013) Proliferation of amyloid- β 42 aggregates occurs through a secondary nucleation mechanism. *Proc Natl Acad Sci USA* 110(24):9758–9763.
25. Cohen SI, Vendruscolo M, Dobson CM, Knowles TP (2012) From macroscopic measurements to microscopic mechanisms of protein aggregation. *J Mol Biol* 421(2–3):160–171.
26. Boehm MF, et al. (1995) Design and synthesis of potent retinoid X receptor selective ligands that induce apoptosis in leukemia cells. *J Med Chem* 38(16):3146–3155.
27. le Maire A, et al. (2012) Retinoid receptors and therapeutic applications of RAR/RXR modulators. *Curr Top Med Chem* 12(6):505–527.
28. Pérez E, Bourguet W, Gronemeyer H, de Lera AR (2012) Modulation of RXR function through ligand design. *Biochim Biophys Acta* 1821(1):57–69.
29. Altucci L, Leibowitz MD, Ogilvie KM, de Lera AR, Gronemeyer H (2007) RAR and RXR modulation in cancer and metabolic disease. *Nat Rev Drug Discov* 6(10):793–810.
30. Ghose AK, Crippen GM (1986) Atomic physicochemical parameters for three-dimensional structure-directed quantitative structure-activity relationships. I. Partition coefficients as a measure of hydrophobicity. *J Comput Chem* 7(4):565–577.
31. Leach AR (2001) *Molecular Modelling: Principles and Applications* (Pearson Education, Essex, UK).
32. Padayachee ER, et al. (2016) Cerebrospinal fluid-induced retardation of amyloid β aggregation correlates with Alzheimer's disease and the APOE ϵ 4 allele. *Brain Res* 1651:11–16.
33. Hellstrand E, Boland B, Walsh DM, Linse S (2010) Amyloid β -protein aggregation produces highly reproducible kinetic data and occurs by a two-phase process. *ACS Chem Neurosci* 1(1):13–18.
34. Arosio P, Cukalevski R, Frohm B, Knowles TP, Linse S (2014) Quantification of the concentration of A β 42 propagons during the lag phase by an amyloid chain reaction assay. *J Am Chem Soc* 136(1):219–225.
35. Delaglio F, et al. (1995) NMRPipe: A multidimensional spectral processing system based on UNIX pipes. *J Biomol NMR* 6(3):277–293.
36. Tetko IV, et al. (2005) Virtual computational chemistry laboratory—design and description. *J Comput Aided Mol Des* 19(6):453–463.
37. McColl G, et al. (2012) Utility of an improved model of amyloid-beta (A β _{1–42}) toxicity in *Caenorhabditis elegans* for drug screening for Alzheimer's disease. *Mol Neurodegener* 7:57.
38. Brenner S (1974) The genetics of *Caenorhabditis elegans*. *Genetics* 77(1):71–94.
39. Solis GM, Petrascheck M (2011) Measuring *Caenorhabditis elegans* life span in 96 well microtiter plates. *J Vis Exp* 49:2496.